

## Effect of surface on defect creation by self-ion bombardment of Si(001)

J. Tarus,\* K. Nordlund, A. Kuronen,<sup>†</sup> and J. Keinonen

Accelerator Laboratory, University of Helsinki, P.O. Box 43, FIN-00014 Helsinki, Finland

(Received 15 April 1998)

We have studied defect formation and defect distributions in silicon under low-energy (25–800 eV) self-bombardment of the  $2 \times 1$  terminated Si(001) surface. We applied the classical molecular dynamics technique and collected statistically significant averages to be able to detect defect production trends in the energy dependence. The number of defects created in implantations was found to be a superlinear function of energy at low energies ( $< 400$  eV) and larger than the defect production in the bulk up to about 1 keV. We have also examined the depth dependence of close-to-surface damage and explored the energy and time dependence of the defect creation mechanisms and the sensitivity of the results to the choice of the model potential. [S0163-1829(98)06239-0]

### I. INTRODUCTION

Recent developments in several branches of research and product development have increased the interest in damage produced on semiconductor surfaces by ion irradiation. For instance, several surface processing methods utilize low-energy ions in aiding surface growth or etching.<sup>1–4</sup> In semiconductor processing the production of ever shallower junctions is soon expected to involve implantation of dopants into layers only a few tens of nanometers deep.<sup>5,6</sup> As recent computer simulations of metals have shown that the effect of surfaces on damage production can in some cases extend roughly 10 nm into the bulk in metals,<sup>7,8</sup> the question arises whether surface effects could be of importance in ultrashallow implantation of semiconductors as well. Although it is clear that heat spikes are not as important in light semiconductors as they are in heavy metals,<sup>9,10</sup> the regime in which surface effects are important in silicon has not been clearly established.

Molecular dynamics (MD) computer simulations are well suited for studying the mechanisms of damage production both in bulk and close to the surface. Use of quantum mechanical methods such as density-functional theory<sup>11</sup> (DFT) and tight binding formalism<sup>12</sup> are currently limited to very small system sizes and time scales. Classical MD simulation techniques with modern interatomic potentials are an efficient and reasonably accurate way to study beam-material interactions<sup>13,14</sup> and can give us the required atomic information of these interactions. In MD simulations the atoms interact via a model potential and the evolution of this ensemble of atoms is followed by solving the equations of motion. Present-day computing power limits system sizes to about  $10^6$  atoms and time scales to nanoseconds. This range of time scales and system sizes is, however, quite adequate for studying the defect creation phase of ion-induced collision cascades. Subsequent defect evolution can be modeled using, e.g., the kinetic Monte Carlo method.<sup>15</sup>

The MD method has been extensively applied in studies of production and annealing of ion-beam induced lattice defects in bulk semiconductors<sup>9,10,16</sup> and ion-beam induced amorphization of silicon.<sup>17–21</sup> The interaction of low-energy ion beams with semiconductor surfaces has also been inves-

tigated using the MD method.<sup>22</sup> Kitabatake *et al.* have performed detailed investigations of bombardment of the Si(001)  $2 \times 1$  surface with Si and In ions in the energy range 10–50 eV.<sup>22–25</sup> In addition to depth distributions of the residual defects remaining immediately after the cascade, they calculated the defect migration energies and minimum energy diffusion paths. The results show that interstitials created during bombardment migrate easily towards the surface while vacancies are less mobile.

Simulations using non-normal incidence of the projectile were performed by Ramana Murty and Atwater.<sup>26</sup> They studied the defect generation during bombardment of the Si(001) surface by 10–50 eV Ar atoms using an angle of incidence of  $45^\circ$  and found that at energies below 20 eV there was considerable displacement of surface atoms but no bulk damage. Hensel and Urbassek<sup>27,28</sup> have examined the effect of (001)  $2 \times 1$ , (110), and (111) Si surfaces on the implantation process of 50 and 100 eV Si atoms. As expected, the surface geometry had a prominent effect on the final depth of the projectile and on the damage distributions.

The present work addresses a few previously unanswered questions regarding defect creation processes close to the silicon (001) surface. Using MD simulations of 25–800 eV recoils in Si and simulating a large number of events in each case we obtain a quantitative, statistically significant picture of the defect creation processes. We examine the question at what energy the damage creation by Si self-recoils becomes bulklike and how the surface affects the processes close to the damage creation threshold energy. We determine the depth dependence of close-to-surface damage, explore the energy and time dependence of the defect creation mechanisms and the sensitivity of the results to the choice of the model potential.

This paper is organized as follows. The computational details of our simulations will be presented in Sec. II. The results will be given in Sec. III and discussed in Sec. IV. We conclude in Sec. V.

### II. COMPUTATIONAL DETAILS

#### A. Potential

The quality of results obtained in MD simulations depends on the quality of the model potential used. In the case

of metals the embedded atom method seems to provide a rather successful approach for describing a large variety of nonelectronic properties.<sup>29</sup> In the case of semiconductors the situation is not as satisfactory. For silicon there are many model potentials that give a good description of some properties, but none of them can be considered superior to the others.<sup>30</sup>

In this work we used the Tersoff many-body potential. This potential was chosen because it is fitted, in addition to the diamond structure, to over- and undercoordinated configurations and thus is expected to give a fairly good description of collision cascades. There are two different parametrizations for this particular potential.<sup>31,32</sup> Both of these parametrizations give a quite good description of the Si(001)  $2 \times 1$  surface,<sup>30</sup> but since the latter one<sup>31</sup> describes the elastic properties better and is thus better suited for cascade studies, it was used in these simulations.

One problem with the Tersoff potential (and generally with most semiempirical potentials) is that it is fitted to the near-equilibrium states and thus does not give realistic description of repulsive interactions that play a significant role in ion-solid interactions. To realistically treat these atomic interactions at small distances, we calculated a repulsive potential with the program package DMOL,<sup>33</sup> which is based on the density-functional theory.<sup>34,35</sup> The repulsive and attractive potentials were smoothly joined together using a Fermi function  $F(r) = (1 + e^{-b_f(r-r_f)})^{-1}$  and the values  $b_f = 12 \text{ \AA}^{-1}$  and  $r_f = 1.6 \text{ \AA}$  for the fitting parameters. These parameters were chosen so that the potential remained smooth in both a dimer and a bulk case and the alteration only affected the repulsive part of the potential.

One has to keep in mind that the semiempirical model potential has many limitations and shortcomings and thus is probably the main error source in these calculations. The potential has been found to give wrong defect energies and a wrong melting point, which probably affects the recombination of defects and recrystallization of the lattice. Consequently, the results presented may not be quantitatively accurate, but we feel that the qualitative results can still elucidate damage production mechanisms in silicon.

### B. Displacement energy and cascade simulations

In the bulk displacement energy calculations the size of the simulation cell was  $7 \times 7 \times 7$  unit cells (2744 atoms) with periodic boundary conditions in three dimensions and the  $x$  and  $y$  sides fixed. For the surface displacement energy a  $6 \times 6 \times 6$  box (1728 atoms) with a reconstructed surface (as explained in Sec. III A) was used. In these simulations a lattice atom was given initial momentum along the  $\langle 001 \rangle$  direction and the evolution of the system was followed until a stable configuration within the time scale used was found.

In the cascade simulations the size of the simulation box ranged from  $6 \times 6 \times 6$  unit cells (1728 atoms) to  $14 \times 14 \times 18$  unit cells (28224 atoms). With these cell sizes all defect production processes occurred far from the cell borders. In the surface cascade case we used periodic boundary conditions in two dimensions and fixed bottom atoms. In bulk cascade studies the box was naturally periodic in all three dimensions. The time evolution of the system was followed for 1.5–3.5 ps, after which the temperature of the simulation

box was quenched down by scaling the atomic velocities by a factor of 0.99 at each time step. The atomic velocities near the fixed or periodic borders were scaled towards zero in all the simulations.

We used six different energies, namely, 25, 50, 100, 200, 400, and 800 eV, in the study of ion bombardment of the surface. The starting point of the projectile was generated from the uniform probability distribution over an area with the size of a unit cell side and placed 2 Å above the surface, after which it was given an initial velocity perpendicular to the surface.

In the bulk recoil simulations a lattice atom was given an initial momentum close to the  $\langle 001 \rangle$  direction. To avoid direct head to head collisions the polar angle of the velocity vector (with respect to the  $\langle 001 \rangle$  direction) was varied between  $0^\circ$  and  $15^\circ$  and the azimuthal angle between  $0^\circ$  and  $180^\circ$ .

Even though the electronic stopping power at the energies used is small, it is not negligible. The electronic slowing down was taken into account as a nonlocal friction force affecting atoms with a kinetic energy higher than 5 eV. The electronic stopping power data for silicon is from Ref. 36.

The Smith-Harrison integration algorithm<sup>37</sup> was used with a variable time step<sup>38</sup> using a maximum step limit of 2 fs. The time step was chosen so that no atom moved more than 0.1 Å or the potential energy of an atom was not changed more than 0.36 eV in a step. The temperature of the simulation box was set to 0 K at the beginning of the simulations. This is of course physically unrealistic, but the choice of 0 K as ambient temperature excludes statistical fluctuations that would lead to higher uncertainties in the final results at higher temperatures. The surface damage simulations correspond to the bombardment of noncontaminated silicon surface by neutral silicon atoms in an ultrahigh-vacuum chamber.

### C. Melting point

Local melting phenomena can be an important part of cascade development. The melting point values cited for the Tersoff potential in the literature show great variation.<sup>30,39,40</sup> Morris *et al.* have recently pointed out that conventional approaches of determining the melting point for interatomic potentials from the free energy or by cooling and heating a simulation cell can be quite error prone.<sup>41</sup> They used an intuitively clear method to determine the melting point from MD simulations. By determining the temperature at which a liquid and a solid co-exist in equilibrium in the same simulation cell, one can avoid any chance of undercooling or overheating phenomena.

We determined the melting point of silicon predicted by the Tersoff potential using a cell with 1728 atoms initially in the crystalline phase and 1728 atoms initially in the liquid phase and using a pressure control algorithm<sup>42</sup> to keep the cell at zero pressure throughout the simulation. The GEAR V integration algorithm<sup>43</sup> was applied in this part of the study. We simulated the system at different constant temperatures in the range from 1500 to 3000 K, using visual inspection of the atom positions and monitoring the average potential energy of the atoms to determine whether the cell melted or crystallized at a given temperature.

### D. Defect analysis

There are various methods to detect defects in solids. The presence of the surface makes the use of bonding and potential energy analysis complicated. Hence we have used two geometrical methods to analyze the defects in the sample, namely, the Wigner-Seitz (WS) cell<sup>44</sup> method and a method based on the Lindemann radius.<sup>27,45</sup>

In the WS method a vacancy is identified when a primitive cell of the lattice is empty and an interstitial or interstitials when there is more than one atom in a cell. In this study the WS cells are centered at the atomic positions of the quenched configuration (explained in Sec. III A).

Another way is to use the Lindemann radius, i.e., the amplitude of lattice vibrations of atoms at the melting point. A vacancy is identified if there is no atom within the Lindemann radius from the lattice point. All the atoms outside these spheres are labeled as interstitials. Since the Tersoff potential does not give the right melting temperature the Lindemann radius for the Stillinger-Weber potential was used. This choice also enabled a comparison of current results with those given in Ref. 28.

The difference between these two methods is that the Wigner-Seitz cells are space filling whereas Lindemann spheres are not. The WS method is ideally suited for point defect detection, when the surrounding lattice preserves its initial structure. In contrast, the Lindemann radius method is very sensitive for displacements in the lattice and is therefore suited for detecting the amount of disorder in the lattice.

Many studies have shown that low-energy single silicon atom recoils in crystalline silicon do not produce amorphization,<sup>10,19,46,47</sup> although it has been found that overlapping 200 eV cascades can do so.<sup>46</sup> These results suggest that only point defects or clusters of point defects are produced during the irradiation at low energies. As the energy gets closer to keV energies the probability of amorphous pocket formation rises. Nevertheless, for consistency, all the results were analyzed by the WS method.

In this work an adatom is defined as an atom that is more than half a layer distance but less than 3 Å (which is the cutoff radius for the potential used) above the surface layer. All atoms that are 3 Å or more above the surface are labeled sputtered.

## III. RESULTS

### A. Surface reconstruction

The reconstruction of the surface was carefully studied so that the effect of surface on the ion bombardment would be understood better. The atoms in the surface layer were positioned into a  $2 \times 1$  pattern with the initial dimer bond length set to 2.3 Å. This cell was thermalized by a 500 fs simulation at 300 K to get the atoms relaxed and then quenched to 0 K.

The dimer bond length stabilized at 2.36 Å, which is more or less the same as the bulk bond length. The pair-correlation function for the next layer (layer 1 in Fig. 1) is also different from the bulklike pair-correlation function. This is because the dimer atoms pull the atoms in layer 1 towards themselves. The distance between the the surface and layer 1 is about 0.2 Å narrower than the layer distance in the bulk. In the next two layers one row of atoms is below the dimer row,

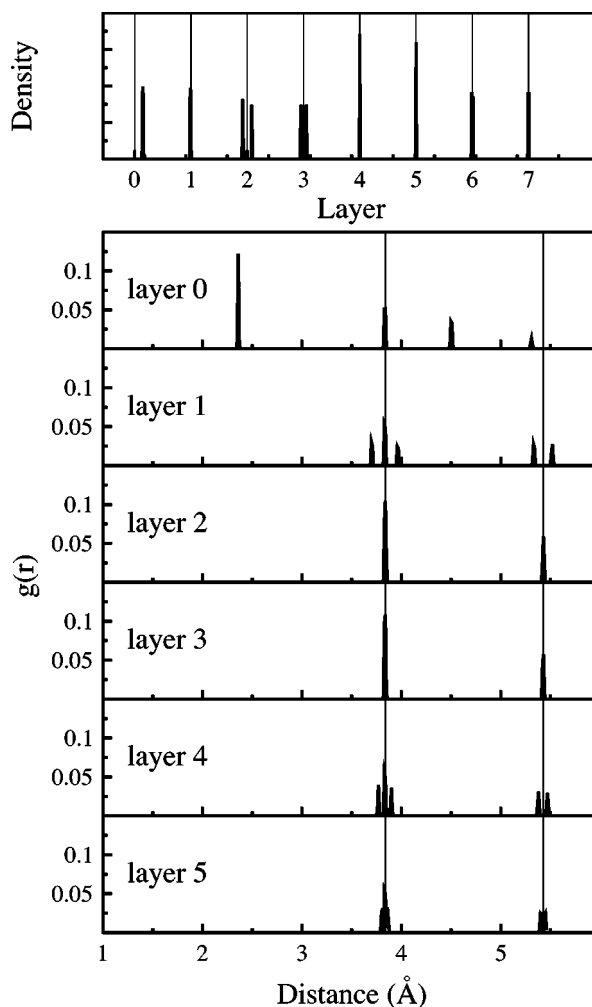


FIG. 1. Surface reconstruction. The surface layer is denoted by zero. Upper part: the longitudinal positions of the layers. The first peak on the left is the surface peak. The narrow lines correspond to the bulklike layer places. Lower part: the pair-correlation functions for different layers. The narrow lines correspond to the bulklike pair-correlation function.

whereas one row is between the dimer rows. The atoms directly below the dimer rows in these layers are pushed into the bulk, whereas the atoms between the dimer rows rise somewhat. In other words, these layers are split. The splitting distance is 0.22 Å in layer 2 and 0.15 Å in layer 3. The atoms in the next two layers (4 and 5) are equivalent with respect to the dimer rows and because of that there is only planar disturbance in these layers. The atom rows move in the opposite direction relative to the surface atom rows. The displacement is only about 0.06 Å in layer 4 and 0.02 Å in layer 5. The split in the next layer (6) is very small, about 0.02 Å. There is no distinguishable disturbance in the layers below. The average potential energies per atom in the layers are given in Table I. Our results agree with the (less detailed) description by Kitabatake *et al.*<sup>22</sup>

### B. Melting point

The time development of the average potential energy at a given initial temperature can be seen in Fig. 2. A rising curve corresponds to melting and a falling one to the recrystalliza-

TABLE I. Potential energies in different atom layers for the Si(001) surface. The surface layer is denoted by zero.

| Layer     | Potential energy (eV) |
|-----------|-----------------------|
| 0         | -3.549                |
| 1         | -4.378                |
| 2 (upper) | -4.609                |
| 2 (lower) | -4.614                |
| 3 (upper) | -4.619                |
| 3 (lower) | -4.618                |
| 4         | -4.626                |
| 5         | -4.630                |
| 6         | -4.629                |
| 7         | -4.630                |
| bulk      | -4.630                |

tion of the lattice. The results indicate that the melting point of silicon with the Tersoff potential is  $2450 \pm 50$  K. To confirm that the interface effects do not affect the result, some of the simulations were repeated with a system size of 16 000 atoms. The larger system gave the same result as the smaller one. We also verified that the joining of the high-energy repulsive potential did not affect the result.

### C. Displacement energy

Even though the bulk displacement threshold energy with the Tersoff potential has already been studied quite thoroughly,<sup>48</sup> we will present our results in order to set a basis for comparison with surface displacement threshold energy simulations. As already explained, a lattice atom was given an initial momentum and the evolution of the system was followed until an equilibrium configuration was reached. The distances between the initial and final place of the recoil atoms are shown in Fig. 3. A close vacancy-interstitial pair, separated by  $2.35 \text{ \AA}$ , was obtained to be formed at  $9.9 \text{ eV}$  and a replacement process to take place at  $15.6 \text{ eV}$ . Nevertheless, at some energies between those values the recoil atom returned to its initial site and thus the energy of  $15.6 \text{ eV}$  should be considered as the real threshold displacement energy.

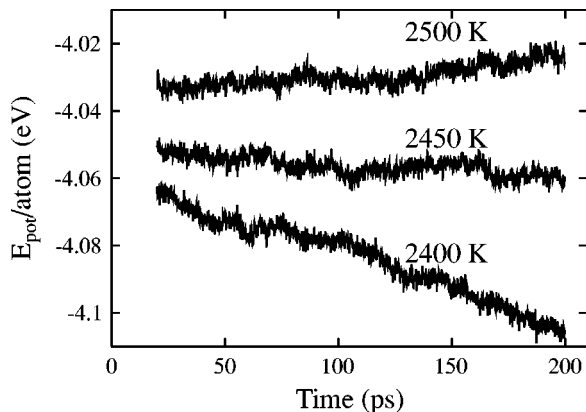


FIG. 2. Time evolution of the potential energy in the melting study. A rising curve corresponds to melting and a falling one to the recrystallization of the lattice.

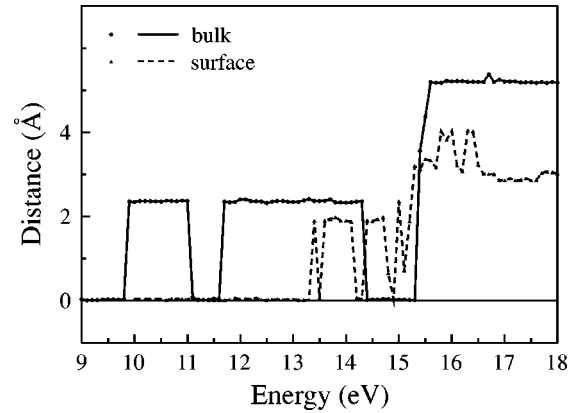


FIG. 3. Distance between the final and initial sites of a recoil atom in the bulk and surface threshold displacement energy studies.

The situation is somewhat different on the surface than in the bulk. The surface atom has fewer bonds and the vicinity of the surface also enables easier deformation of the lattice. Nevertheless, because of the surface reconstruction the  $\langle 001 \rangle$  direction is not similarly open as it is in the bulk. Because of this reconstruction we see no close tetrahedral interstitial configuration on the surface until  $13.4 \text{ eV}$ . A split dumbbell was obtained to be formed at  $15.3 \text{ eV}$  and a replacement process takes place at  $15.8 \text{ eV}$ .

Thus we see that a close vacancy-interstitial pair can be formed at lower energies in the bulk than on the surface. Nevertheless, a replacement process seems to take place in both cases at about same energy.

### D. Surface damage

In order to get statistically satisfactory results, around 100 recoil events were calculated for most energies. The defects were detected after every ten time steps by the two methods described in Sec. II D.

The average defect numbers detected by the WS method as a function of time for the  $100 \text{ eV}$  case can be seen in Fig. 4. The vacancy and the interstitial numbers rise rapidly after the projectile hits the target and with energies up to  $200 \text{ eV}$  (Ref. 49) the maximum vacancy and interstitial numbers are reached at about  $0.2 \text{ ps}$ . After that these defects start to recombine and a stable configuration with respect to defect

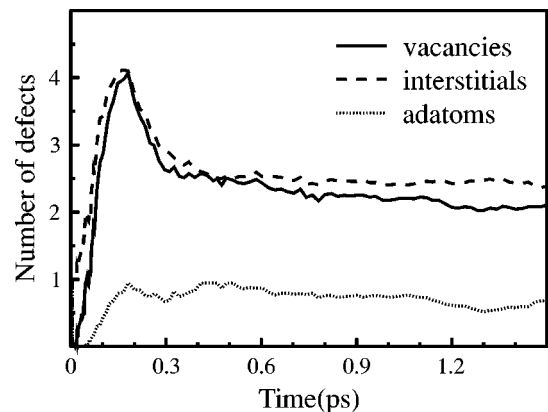


FIG. 4. Time evolution of the average number of vacancies, interstitials, and adatoms during  $100 \text{ eV}$  cascades.

TABLE II. Results for surface cascades. Upper part: the average number of defects per one ion after quenching. Lower part: the number of defects per eV (normalized to the 100 eV case).

| Energy (eV) | Vacancies        | Interstitials    | Adatoms         | Sputtered         |
|-------------|------------------|------------------|-----------------|-------------------|
| 25          | $0.25 \pm 0.05$  | $0.92 \pm 0.05$  | $0.31 \pm 0.05$ | $0.019 \pm 0.013$ |
| 50          | $0.81 \pm 0.08$  | $1.39 \pm 0.06$  | $0.42 \pm 0.06$ | $0.007 \pm 0.007$ |
| 100         | $2.09 \pm 0.15$  | $2.41 \pm 0.10$  | $0.65 \pm 0.08$ | $0.034 \pm 0.017$ |
| 200         | $4.79 \pm 0.17$  | $4.77 \pm 0.13$  | $0.92 \pm 0.12$ | $0.10 \pm 0.03$   |
| 400         | $9.51 \pm 0.36$  | $8.92 \pm 0.30$  | $1.37 \pm 0.19$ | $0.22 \pm 0.06$   |
| 800         | $17.03 \pm 0.43$ | $16.13 \pm 0.37$ | $1.55 \pm 0.21$ | $0.35 \pm 0.08$   |
| 25          | 0.48             | 1.53             | 1.91            | 2.24              |
| 50          | 0.78             | 1.15             | 1.29            | 0.41              |
| 100         | 1                | 1                | 1               | 1                 |
| 200         | 1.14             | 0.99             | 0.71            | 1.47              |
| 400         | 1.13             | 0.92             | 0.53            | 1.62              |
| 800         | 1.02             | 0.84             | 0.30            | 1.29              |

development is achieved at about 0.5 ps. The behavior of adatoms is somewhat different. The number of adatoms begins to rise after 0.05 ps and reaches the maximum value at 0.5 ps, i.e., at the same time when the vacancy and interstitial numbers become stable. It seems that there is no significant recombination of the surface vacancies and adatoms since the adatom number never reduces drastically. The number of defects was not changed significantly after the quenching.

The average numbers of defects per ion after the quenching are presented in Table II. It can be seen that the production of vacancies is a superlinear function of energy below 400 eV (see Fig. 5), i.e., the number of vacancies per eV is higher at higher ion energies. This superlinearity extends to much higher energies than what is expected on the basis of the Kinchin-Pease formula.<sup>50</sup> At energies below 50 eV, the comparison of the energy dependence is not relevant since the energy in the Kinchin-Pease formula is the energy of a recoiling lattice atom, whereas in the MD simulations it is the energy of an ion intruding on the surface.

The average number of defects detected by the WS and Lindemann methods during a 100 eV collision cascade can be seen in Fig. 6. The peak number of defects is reached at

the same time by both methods. At that time the number of vacancies detected by the Lindemann method is 10.5 times greater than by the WS method. That indicates that on average 43 atoms (excluding sputtered and adatoms) are disordered during a 100 eV irradiation. After quenching the Lindemann vacancy number is only 5.5 times bigger than the WS vacancy number. The difference is similar with energies up to 200 eV.<sup>49</sup> Once more we emphasize that the defects detected by the Lindemann method are not the number of point defects but the amount of disordering in the lattice.

### E. Defect distribution in atom layers

The average vacancy and interstitial distributions as a function of atom layers for three different energies are shown in Fig. 7. At low energies ( $\leq 200$  eV) the interstitial distribution is much wider than the vacancy distribution, whereas at higher energies the vacancy distribution closes in on the interstitial distribution. In all the cases the vacancy number is highly peaked at the surface layer, but the percentage of vacancies in the surface layer relative to all the vacancies drops from 73% (at 25 eV) to 6.6% (at 800 eV) as the energy rises. The peak value of the interstitial distribution is close to the ion penetration mean depth (see Table III).

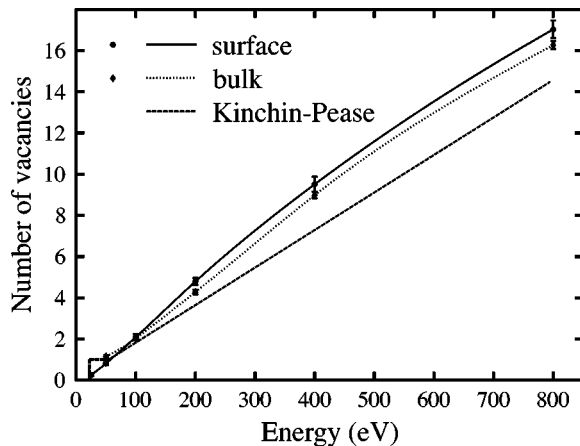


FIG. 5. Average number of vacancies for surface and bulk cascades and the Kinchin-Pease formula prediction. The Kinchin-Pease slope was determined from the slope between the 400 and 800 eV bulk points. The lines are drawn to guide the eye.

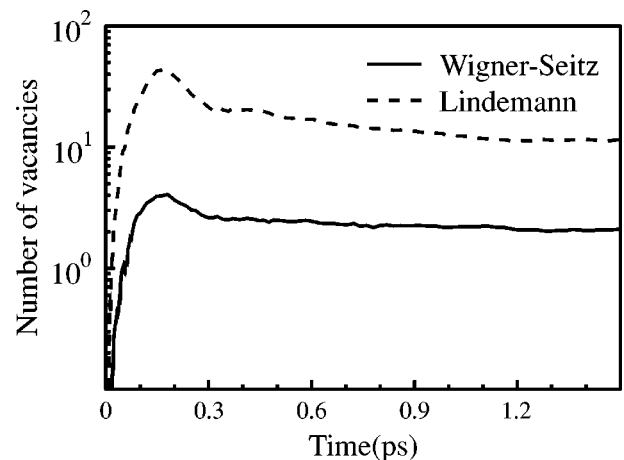


FIG. 6. Average number of vacancies detected by Wigner-Seitz cell and Lindemann radius methods in 100 eV cascades.

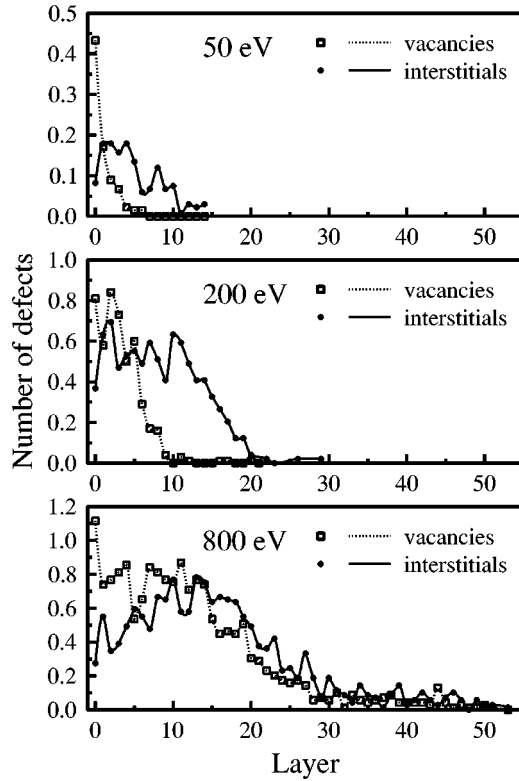


FIG. 7. Defect probability distribution over the layers for 50, 200, and 800 eV recoils. The surface is layer 0. The lines are drawn to guide the eye.

The time evolution of the vacancy depth distribution at 100 eV is shown in Fig. 8. At 0.078 ps, at the point when the vacancy number is approximately the same as after the quenching, the distribution is almost linear. At the peak point (0.18 ps) the vacancy numbers in the topmost layers have increased significantly. After the quenching the shape of the distribution is more or less the same, only the overall vacancy number has reduced.

#### F. Bulk damage

In order to clarify the influence of the surface in defect formation we also performed 50, 100, 200, 400, and 800 eV bulk cascade studies. The average number of defects produced in these recoils is shown in Table IV. Because in the bulk cascade simulations the initial energy was given to a lattice atom, the defect production at energies below 100 eV is in reasonable agreement with the Kinchin-Pease formula prediction. However, the superlinearity in vacancy produc-

TABLE III. Ion penetration mean depths. Because of the channeling, the ranges above 200 eV increase strongly.

| Energy (eV) | Range (Å)       | Events |
|-------------|-----------------|--------|
| 25          | $0.71 \pm 0.13$ | 103    |
| 50          | $1.61 \pm 0.14$ | 134    |
| 100         | $2.38 \pm 0.10$ | 116    |
| 200         | $4.49 \pm 0.22$ | 100    |
| 400         | $11.1 \pm 0.7$  | 49     |
| 800         | $25.5 \pm 2.5$  | 69     |

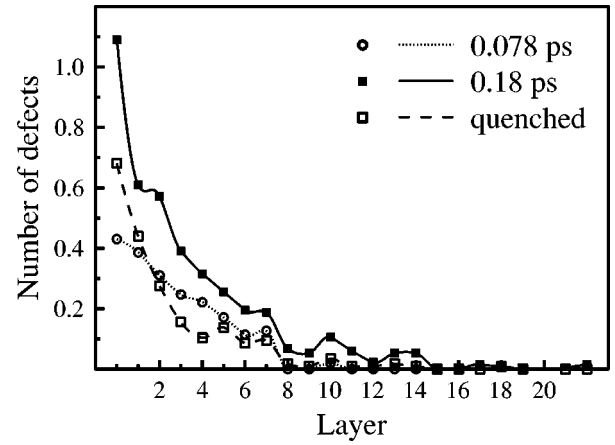


FIG. 8. Time evolution of the vacancy number in different atom layers for 100 eV irradiation.

tion continues to a much higher energy (to about 400 eV) than predicted by the Kinchin-Pease formula.

## IV. DISCUSSION

### A. Melting point

Frequently the high melting point of silicon described by the Tersoff potential has been used as an argument against the suitability of this potential in collision cascade calculations. The actual value of the melting point, however, has not been clearly established. The original paper presenting the potential gave a very inaccurate value of  $3000 \pm 500$  K.<sup>31</sup> Other determinations have given values in the range 2500–3000 K, but the determinations have been typically performed for small system sizes without pressure control or in cases where overheating or undercooling is possible.<sup>30,39,40</sup> Our result,  $2450 \pm 50$  K, while still much higher than the experimental value of 1683 K,<sup>51</sup> is not as unrealistic as the previously determined values. Nevertheless, the wrong melting point affects the final defect numbers at high energies since liquid quenches into an amorphous phase too rapidly.<sup>10</sup> At the energies used in the present work, where large amorphous zones are not formed, this is not a significant problem.

TABLE IV. Damage production in bulk cascades. Upper part: the average number of defects per one ion after quenching. Lower part: the number of defects per eV (normalized to the 100 eV case, as the 50 eV case is strongly affected by the low-energy Frenkel pair production).

| Energy (eV) | Vacancies        | Interstitials    | Events |
|-------------|------------------|------------------|--------|
| 50          | $1.15 \pm 0.04$  | $1.15 \pm 0.04$  | 120    |
| 100         | $2.02 \pm 0.07$  | $2.02 \pm 0.07$  | 105    |
| 200         | $4.28 \pm 0.11$  | $4.28 \pm 0.11$  | 120    |
| 400         | $8.98 \pm 0.15$  | $8.98 \pm 0.15$  | 59     |
| 800         | $16.27 \pm 0.19$ | $16.27 \pm 0.19$ | 49     |
| 50          | 1.14             | 1.14             |        |
| 100         | 1                | 1                |        |
| 200         | 1.06             | 1.06             |        |
| 400         | 1.11             | 1.11             |        |
| 800         | 1.01             | 1.01             |        |

### B. Displacement energy

The threshold energy for an atomic displacement in silicon has been studied extensively both experimentally<sup>52–55</sup> and using computer simulations.<sup>56–59</sup> Nevertheless, the data are quite dispersed. The experimental values for the displacement energy lie between 11 and 30 eV and computer simulation data between 10 and 22 eV.

Sayed *et al.* have done a simulation study of displacement energies in silicon using the Tersoff potential.<sup>59</sup> They have determined the threshold energy in the  $\langle 001 \rangle$  direction to be 10 eV. Another study done by Caturla *et al.*<sup>57</sup> gave the value of 22 eV with the Stillinger-Weber potential. The difference between predicted displacement energies can partially be explained by different configurations produced. With the Tersoff potential a neighboring tetrahedral interstitial is formed at 9.9–15.5 eV, whereas a replacement process takes place at energies of 15.6 eV or higher. Nevertheless, the close tetrahedral interstitial configuration was found to be a metastable configuration. In some cases the vacancy and the interstitial recombine. With the Stillinger-Weber potential no stable (or metastable) neighboring interstitial-vacancy pair is observed for low-energy recoils.<sup>57</sup> The Frenkel pair is produced only through a replacement process. This is probably due to the fact that the Stillinger-Weber potential is fitted only to the tetrahedral configuration and thus penalizes nontetrahedral bonding types. The stiffness of this potential has also been found to be too large when comparing it to the tight-binding method.<sup>60</sup>

Some experiments indicate a much higher displacement energy than what is predicted by our simulations. When comparing these results one should note that close Frenkel pairs in Si have been shown to anneal at temperatures of only 10–50 K.<sup>61</sup> Most experimental studies of the threshold displacement energy have been carried out at higher temperatures. Also, recent tight-binding calculations suggest that close Frenkel pairs can under some circumstances recombine spontaneously or form a metastable bond defect complex.<sup>62,63</sup> Therefore, the closest interstitial-vacancy pairs seen in our simulations (created at the lowest recoil energies) may not exist adequately long to be visible in experiments, which may explain why the experimental values for the displacement threshold energy tend to be higher than our simulated ones. Nevertheless, as the lifetime of such configurations, according to our simulations, seems to be at least of the order of picoseconds, they may influence the evolution of collision cascades and thus defect production during ion irradiation.

### C. Surface damage

As noted already, the defect production is a superlinear function of energy at energies below 400 eV, but becomes linear at higher energies. The linear dependence at keV energies has been observed previously.<sup>10</sup> The reason behind this linearity could be that collision cascades in silicon separate into subcascades. The higher the energy is, the more subcascades are formed. At low energies, however, no distinct subcascades form. The growth of one cascade could be the reason for the superlinearity at low energies.

The Lindemann results are compared to those given by Hensel and Urbassek,<sup>28</sup> where the same analysis of the de-

fects was used. They used the Stillinger-Weber potential to describe the bonding in silicon. The number of vacancies obtained by Hensel and Urbassek is for 50 eV bombardment about 40% and for 100 eV bombardment about 30% higher than what was obtained in our simulations. This could be due to the fact that the vacancy formation energy is somewhat lower with the Stillinger-Weber potential (2.82 eV) than with the Tersoff potential (3.70 eV).<sup>30</sup> DFT calculations give values between 3 and 4 eV.<sup>30</sup> Nevertheless, as noted earlier, the Lindemann radius method gives the amount of disorder in the lattice, not the number of point defects. The larger disordering with the Stillinger-Weber potential could again rise from the stiffness of the potential. The lattice around defects could be more disordered than with the Tersoff potential as the Stillinger-Weber potential tries to affix all the atoms with four bonds. According to our tests with the Stillinger-Weber potential, the Lindemann method gives three vacancies for a single dumbbell-interstitial configuration.

### D. Defect distribution in atom layers

The results presented in Sec. III suggest that at the early stage of the cascade, vacancies close to the surface migrate towards it, leading to a high number of surface layer vacancies. After the peak point the evolution seems to be governed by the recombination of vacancies and interstitials and thus the vacancy number drops.

As we look at the defect distribution at the lowest energy (25 eV) we see that it is very shallow. This suggests that even spontaneous annealing of the lattice is possible and thus this energy would be well suited for ion beam epitaxy (IBE). The growth of crystalline layers is achieved more easily when the defect distribution is low and located in a shallow area. This is also in agreement with experimental results, where an optimal energy value of  $20 \pm 10$  eV has been found to be ideal for IBE.<sup>64</sup>

The 50 eV case has also been studied by Kitabatake and Greene.<sup>25</sup> The overall defect production is somewhat lower in our study than in theirs. The average number of interstitials in their study was 1.8, to be compared with 1.39 in ours (see Table II). As no statistical error is given to their results, we cannot deduce whether the difference is due to our modification of the potential (corrected repulsive part) or due to statistical error. Nevertheless, the statistics in our study is much better (134 vs 36 incident ions). Moreover, the 36 cases calculated by Kitabatake and Greene do not represent a random sampling of impact points on the Si surface. The ion range is more or less the same in both studies.

### E. Surface and bulk damage comparison

The comparison of surface and bulk defects at low energies is somewhat complicated. In the surface case an extra atom is introduced into the lattice, whereas in the bulk a lattice atom is removed from its lattice site. Furthermore, in the surface case the impact point is chosen randomly, whereas in the bulk the recoil atom always originates in the same point. We attempted to minimize this difference by giving the bulk recoil atom random angles along the  $\langle 001 \rangle$  direction.

Despite the problems, we can conclude that in the surface bombardment the defect production is somewhat affected by

the surface at least up to an energy of 1 keV. This is, of course, expected as a large portion of vacancies is produced in the surface layer and the bond energy of a surface atom is significantly lower than that of a bulk atom. However, the difference is less than 10% at energies above 400 eV, in clear contrast to what has been obtained for metals, where surfaces can have a dramatic effect on damage production up to energies of at least 10 keV.<sup>7</sup>

## V. CONCLUSIONS

We have studied the mechanisms that produce damage on and close to the silicon (001) surface using classical molecular dynamics simulations of atomic collision processes. We simulated a large number of events in each case to obtain a reliable quantitative picture of defect creation mechanisms.

Since local melting phenomena are an important part of cascade development, we determined the melting point of Si modeled by the Tersoff potential. Using a pressure control scheme and a liquid-solid interface we determined the melting point to be  $2450 \pm 50$  K. This is lower than previous calculations have indicated.

To understand the fundamental mechanisms of damage creation during ion irradiation we studied the displacement

processes in bulk and surface layers in detail. We found that the surface strongly affects both the threshold displacement energy and damage creation mechanism. At energies between 10 and 15 eV a very close vacancy-interstitial pair can be formed in the bulk and above 15.5 eV a replacement process takes place. Because of the reconstruction, the threshold energy for close pair formation at the surface is higher, above 13 eV. As in the bulk, replacementlike processes start to occur around 15.5 eV.

We also studied the defect creation in cascades at the near surface region under low-energy self-ion bombardment of the  $2 \times 1$  terminated Si(001) surface and compared the results to bulk cascades at the same energies. We showed that there is a weak superlinearity in the vacancy production for low energy ( $< 400$  eV) recoils. Furthermore, the depth distribution of defects was found to be significantly greater than the ion penetration depth. The vacancy distribution was at all energies peaked in the dimer reconstructed surface atom layer. When comparing the vacancy and interstitial production in the surface and bulk cascades we found that the surface numbers are somewhat higher. The difference decreases rapidly with energy, being less than 20% at 100 eV and only about 5% at 800 eV.

\*Electronic address: Jura.Tarus@Helsinki.fi

<sup>†</sup>Present address: Laboratory of Computational Engineering, Helsinki University of Technology, P.O. Box 9400, FIN-02015 HUT, Finland.

<sup>1</sup>M.-A. Hasan, J. Knall, S. A. Barnett, J.-E. Sundgren, L. C. Market, A. Rackett, and J. E. Greene, *J. Appl. Phys.* **65**, 172 (1989).

<sup>2</sup>D. Marton, in *Low Energy Ion-Surface Interactions, Wiley Series in Ion Chemistry and Physics*, edited by J. W. Rabalais (John Wiley & Sons, Chichester, 1994), Chap. 9.

<sup>3</sup>T. Matsuura, J. Murota, and Y. Sawada, *Appl. Phys. Lett.* **63**, 2803 (1993).

<sup>4</sup>H. Feil and J. Dieleman, *J. Appl. Phys.* **74**, 1303 (1993).

<sup>5</sup>Y. Taur, Y.-J. Mii, D. J. Frank, H.-S. Wong, D. A. Buchanan, S. J. Wind, S. A. Rishton, G. A. Sai-Halasz, and E. J. Nowak, *IBM J. Res. Dev.* **39**, 245 (1995).

<sup>6</sup>D. F. Downey, C. M. Osburn, and S. D. Marcus, *Solid State Technol.* **40**, 71 (1997).

<sup>7</sup>M. Ghaly and R. S. Averback, *Phys. Rev. Lett.* **72**, 364 (1994).

<sup>8</sup>Y. Zhong, K. Nordlund, M. Ghaly, and R. S. Averback, *Phys. Rev. B* **58**, 2361 (1998).

<sup>9</sup>T. Diaz de la Rubia, *Nucl. Instrum. Methods Phys. Res. B* **120**, 19 (1996).

<sup>10</sup>K. Nordlund, M. Ghaly, R. S. Averback, M. Caturla, T. Diaz de la Rubia, and J. Tarus, *Phys. Rev. B* **57**, 7556 (1998).

<sup>11</sup>R. O. Jones and O. Gunnarsson, *Rev. Mod. Phys.* **61**, 689 (1989).

<sup>12</sup>Y. P. Feng, C. K. Ong, H. C. Poon, and D. Tománek, *J. Phys.: Condens. Matter* **21**, 4345 (1997), and references therein.

<sup>13</sup>R. Smith, M. Jakas, D. Ashworth, B. Owen, M. Bowyer, I. Chakarov, and R. Webb, *Atomic and Ion Collisions in Solids and at Surfaces* (Cambridge University Press, Cambridge, 1997).

<sup>14</sup>W. Eckstein, *Computer Simulations of Ion-Solid Interactions* (Springer-Verlag, Berlin, 1991).

<sup>15</sup>M. Jaraiz, G. H. Gilmer, J. M. Poate, and T. Diaz de la Rubia, *Appl. Phys. Lett.* **68**, 409 (1996).

<sup>16</sup>M.-J. Caturla, T. Diaz de la Rubia, L. A. Marqués, and G. H. Gilmer, *Phys. Rev. B* **54**, 16 683 (1996).

<sup>17</sup>T. Diaz de la Rubia and G. H. Gilmer, *Phys. Rev. Lett.* **74**, 2507 (1995).

<sup>18</sup>M.-J. Caturla, T. Diaz de la Rubia, and G. H. Gilmer, *J. Appl. Phys.* **77**, 3121 (1995).

<sup>19</sup>L. J. Lewis and R. M. Nieminen, *Phys. Rev. B* **54**, 1459 (1996).

<sup>20</sup>T. Motooka, S. Harada, and M. Ishimaru, *Phys. Rev. Lett.* **78**, 2980 (1997).

<sup>21</sup>K. Nordlund and R. S. Averback, *Phys. Rev. B* **56**, 2421 (1996).

<sup>22</sup>M. Kitabatake, P. Fons, and J. E. Greene, *J. Vac. Sci. Technol. A* **8**, 3726 (1990).

<sup>23</sup>M. Kitabatake, P. Fons, and J. E. Greene, *J. Vac. Sci. Technol. A* **9**, 91 (1991).

<sup>24</sup>M. Kitabatake and J. E. Greene, *J. Appl. Phys.* **73**, 3183 (1993).

<sup>25</sup>M. Kitabatake and J. E. Greene, *Thin Solid Films* **272**, 271 (1996).

<sup>26</sup>M. V. Ramana Murty and H. A. Atwater, *Phys. Rev. B* **45**, 1507 (1992).

<sup>27</sup>H. Hensel and H. M. Urbassek, *Radiat. Eff. Defects Solids* **142**, 297 (1997).

<sup>28</sup>H. Hensel and H. M. Urbassek, *Phys. Rev. B* **57**, 4756 (1998).

<sup>29</sup>M. S. Daw, S. M. Foiles, and M. I. Baskes, *Mater. Sci. Rep.* **9**, 251 (1993).

<sup>30</sup>H. Balamane, T. Halicioglu, and W. A. Tiller, *Phys. Rev. B* **46**, 2250 (1992).

<sup>31</sup>J. Tersoff, *Phys. Rev. B* **38**, 9902 (1988).

<sup>32</sup>J. Tersoff, *Phys. Rev. B* **37**, 6991 (1988).

<sup>33</sup>DMOL is a trademark of Bio Sym. Inc., San Diego, CA.

<sup>34</sup>J. Delley, *J. Chem. Phys.* **92**, 508 (1990).

<sup>35</sup>K. Nordlund, N. Runeberg, and D. Sundholm, *Nucl. Instrum. Methods Phys. Res. B* **132**, 45 (1997).

<sup>36</sup>J. Keinonen, K. Arstila, and P. Tikkanen, *Appl. Phys. Lett.* **60**, 228 (1992).

<sup>37</sup>R. Smith and D. Harrison, *Comput. Phys.* **3**, 68 (1989).

- <sup>38</sup>K. Nordlund, *Comput. Mater. Sci.* **3**, 448 (1995).
- <sup>39</sup>M. Ishimaru, K. Yoshida, T. Kumamoto, and T. Motooka, *Phys. Rev. B* **54**, 4638 (1996).
- <sup>40</sup>S. J. Cook and P. Clancy, *Phys. Rev. B* **47**, 7686 (1993).
- <sup>41</sup>J. R. Morris, C. Z. Wang, K. M. Ho, and C. T. Chan, *Phys. Rev. B* **49**, 3109 (1994).
- <sup>42</sup>H. J. C. Berendsen, J. P. M. Postma, W. F. van Gunsteren, A. DiNola, and J. R. Haak, *J. Chem. Phys.* **81**, 3684 (1984).
- <sup>43</sup>C. W. Gear, *Numerical Initial Value Problems in Ordinary Differential Equations* (Prentice-Hall, Englewood Cliffs, NJ, 1971).
- <sup>44</sup>Since the diamond crystal structure is not a Bravais lattice, the cells centered at the lattice atoms are strictly speaking Voronoy polyhedra. See, e.g., N. W. Ashcroft and N. D. Mermin, *Solid State Physics* (Saunders, Philadelphia, 1976), Chap. 4.
- <sup>45</sup>F. A. Lindemann, *Phys. Z.* **11**, 609 (1910).
- <sup>46</sup>D. M. Stock, G. H. Gilmer, M. Jaraíz, and T. Diaz de la Rubia, *Nucl. Instrum. Methods Phys. Res. B* **102**, 207 (1995).
- <sup>47</sup>J. Weber, D. M. Stock, K. Gärtner, and C. Wende, *Radiat. Eff. Defects Solids* **142**, 161 (1997).
- <sup>48</sup>L. A. Miller, D. K. Brice, A. K. Prinja, and S. T. Pricraux, *Phys. Rev. B* **49**, 16 953 (1994).
- <sup>49</sup>The time evolution of defects is not available for 400 and 800 eV surface and bulk cascades because for these simulations we used a code that did not generate this output.
- <sup>50</sup>P. Sigmund, *Appl. Phys. Lett.* **14**, 114 (1969).
- <sup>51</sup>N. W. Ashcroft and N. D. Mermin, *Solid State Physics* (Saunders College Publishing, Philadelphia, 1988).
- <sup>52</sup>J. H. Cahn, *J. Appl. Phys.* **30**, 1310 (1959).
- <sup>53</sup>P. L. F. Hemmet and P. R. C. Stevens, *J. Appl. Phys.* **40**, 4893 (1969).
- <sup>54</sup>J. J. Loferski and P. Rappaport, *J. Appl. Phys.* **30**, 1296 (1959).
- <sup>55</sup>D. Marton, in *Low Energy Ion-Surface Interactions*, edited by J. W. Rabalais (Wiley, Chichester, 1994), p. 526.
- <sup>56</sup>L. Miller, D. Brice, A. Prinja, and T. Pricraux, in *Defects in Materials*, edited by P. D. Bristowe, I. E. Epperson, I. E. Griffith, and Z. Liliental-Weber, MRS Symposia Proceedings No. 209 (Materials Research Society, Pittsburgh, 1991), p. 171.
- <sup>57</sup>M.-J. Caturla, T. Diaz de la Rubia, and G. H. Gilmer, in *Materials Synthesis and Processing Using Ion Beams*, edited by R. I. Culbertson, O. W. Holland, K. S. Jones, and K. Maex, MRS Symposia Proceedings No. 316 (Materials Research Society, Pittsburgh, 1994), p. 141.
- <sup>58</sup>L. Miller, D. Brice, A. Prinja, and T. Pricraux, *Radiat. Eff. Defects Solids* **129**, 127 (1994).
- <sup>59</sup>M. Sayed, J. H. Jefferson, A. B. Walker, and A. G. Cullis, *Nucl. Instrum. Methods Phys. Res. B* **102**, 232 (1995).
- <sup>60</sup>H. Hensel, P. Klein, H. M. Urbassek, and T. Frauenheim, *Phys. Rev. B* **53**, 16 497 (1996).
- <sup>61</sup>P. Ehrhart and H. Zillgen, in *Defects and Diffusion in Silicon Processing*, edited by T. Diaz de la Rubia and S. Coffa, MRS Symposia Proceedings No. 469 (Materials Research Society, Pittsburgh, 1997), p. 175.
- <sup>62</sup>M. Tang, L. Colombo, J. Zhu, and T. Diaz de la Rubia, *Phys. Rev. B* **55**, 14 279 (1997).
- <sup>63</sup>F. Cargnoni, C. Gatti, and L. Colombo, *Phys. Rev. B* **57**, 170 (1997).
- <sup>64</sup>J. W. Rabalais, A. H. Al-Bayati, K. J. Boyd, D. Marton, J. Kulik, Z. Zhang, and W. K. Chu, *Phys. Rev. B* **53**, 10 781 (1996).